Anti-Biofouling and Self-Cleaning Surfaces Featured with Magnetic Artificial Cilia

Zhang, Shuaizhong; Zuo, Pan; Wang, Ye; Onck, Patrick R; den Toonder, Jaap M J

Published in:
ACS Applied Materials & Interfaces

DOI:
10.1021/acsami.0c05403

Publication date:
2020

ACS APPLIED MATERIALS & INTERFACES

www.acsami.org

Research Article

Anti-Biofouling and Self-Cleaning Surfaces Featured with Magnetic Artificial Cilia

Shuaizhong Zhang, Pan Zuo, Ye Wang, Patrick Onck, and Jaap M. J. den Toonder*

Cite This: *ACS Appl. Mater. Interfaces* 2020, 12, 27726–27736

Read Online

ACCESS | Metrics & More | Article Recommendations | Supporting Information

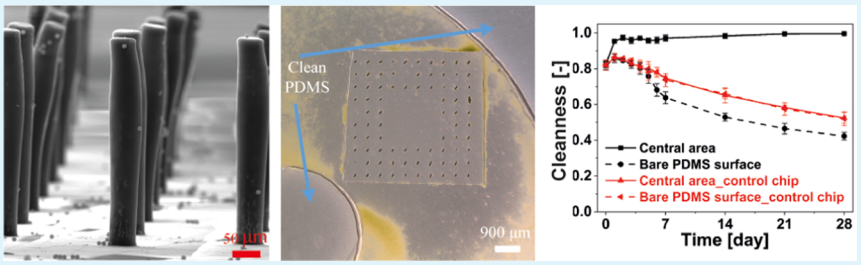

ABSTRACT: The fouling of surfaces submerged in a liquid is a serious problem for many applications including lab-on-a-chip devices and marine sensors. Inspired by the versatility of cilia in manipulating fluids and particles, it is experimentally demonstrated that surfaces partially covered with magnetic artificial cilia (MAC) have the capacity to efficiently prevent attachment and adhesion of real biofouling agents—microalgae *Scenedesmus* sp. Actuation of the MAC resulted in over 99% removal of the algae for two different scenarios: (1) actuating the MAC immediately after injecting the algae into a microfluidic chip, demonstrating antifouling and (2) starting to actuate the MAC 1 week after injecting the algae into the chip and leaving them to grow in static conditions, showing self-cleaning. It is shown that the local and global flows generated by the actuated MAC are substantial, resulting in hydrodynamic shear forces acting on the algae, which are likely to be key to efficient antifouling and self-cleaning. These findings and insights will potentially lead to novel types of self-cleaning and antifouling strategies, which may have a relevant practical impact on different fields and applications including lab-on-a-chip devices and water quality analyzers.

KEYWORDS: *biofouling, anti-biofouling, self-cleaning, magnetic artificial cilia, lab-on-a-chip*

1. INTRODUCTION

Fouling is the accumulation of undesired contaminants such as organic molecules, cells, and microparticles on a submerged surface. Specifically, marine biofouling is the colonization by a vast variety of marine organisms in four chronological phases:[1−6] (1) adsorption of organic molecules that form a conditioning layer; (2) primary colonization by unicellular microorganisms such as microalgae, diatoms, and protozoa, forming a "slime" film; (3) "soft macrofouling" consisting mainly of macroscopically visible algae (seaweeds) and invertebrates; and (4) "hard macrofouling" of shelled invertebrates such as barnacles, mussels, and tubeworms. This indicates that the prevention of the formation of the "slime" film will probably deter fouling.[1] Fouling forms serious problems to diverse applications including (i) biomedical and microfluidic devices, as the adsorption of microparticles, cells, or molecules to the device walls inhibits the normal operation of these devices;[7] (ii) micro-to macroscale sensors present, for example, in oceans, rivers, or lakes for environmental sensing or in chemical and food processing operations, where fouling leads to reduced efficiency and/or operating-lifetime and higher maintenance cost;[8] (iii) off-shore structures and ship hulls, as the buildup of a layer of marine biofouling organisms increases the drag on the ship and hence the fuel consumption.[9,10] In addition to economic loss, biofouling of the hull of intercontinental ships also causes the spread and invasion of nonindigenous marine species into the global ecosystems.[11−14] Thus, the design of surfaces that prevent fouling and are self-cleaning is critical to the viability of a wide range of applications and industries. Especially, the first phases of fouling which can start soon after submersion should be targeted, as it prevents further escalation. For ship hulls, this initial fouling process mainly occurs when the ships are stationary in ports.[1−6]

To date, there are several strategies to design and make anti-fouling surfaces, based on chemical or physical mechanisms, which, however, cannot deter the settlement and attachment of the whole vast variety of biofouling agents.[1,2,7,15] On the other hand, classical microfluidic chip cleaning protocols are tedious

Received: March 23, 2020
Accepted: June 1, 2020
Published: June 1, 2020

https://dx.doi.org/10.1021/acsami.0c05403
ACS Appl. Mater. Interfaces 2020, 12, 27726−27736

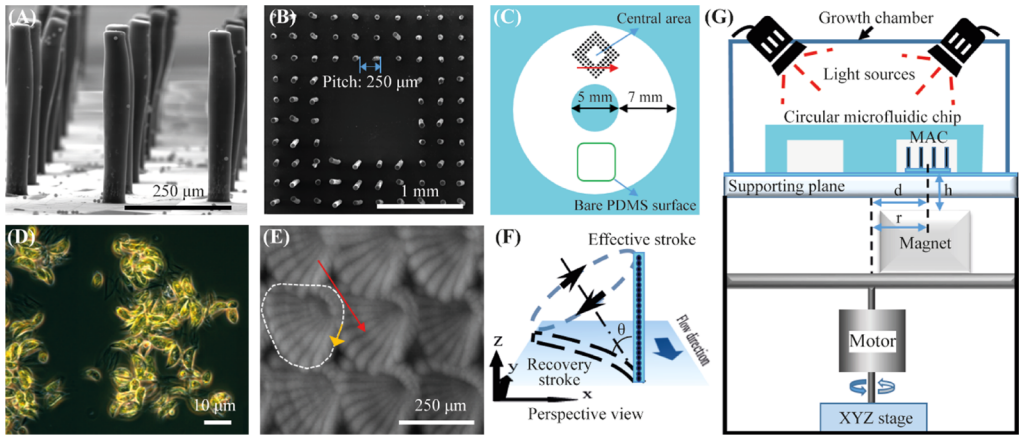

Figure 1. Experimental system. (A) Side-view SEM image of the fabricated MAC with a diameter, height, and pitch of 50, 350, and 250 μm, respectively. (B) Top-view SEM image of the ciliated surface, which consists of a central unciliated area surrounded by three rows of MAC, termed the "partially ciliated surface". The MAC have a pitch of 250 μm. (C) Schematic drawing of the circular microfluidic chip integrated with the partially ciliated surface, indicating the location of the ciliated surface area and the observation areas: central area and bare PDMS surface. The height of the chip is 2 mm. The red arrow denotes the direction of the effective stroke of the cilia motion. (D) Microscopy image of the used algae, *Scenedesmus* sp., which have a crescent shape with an average length of 12 μm and an average width of 4.6 μm. (E) Top-view image of the motion of the rotating MAC at 40 Hz in water. The image is composed of 25 overlapping frames in one actuation cycle. The white dashed line indicates the cilia tip trajectory projected on the surface plane, the orange arrow indicates the rotation direction of the MAC, and the red arrow indicates the direction of the effective stroke. (F) Schematic drawing of the rotating cilium performing a tilted conical motion in perspective view, with an opening angle $\theta = 72°$. Illustration is not to scale. Reproduced with permission.[41] Copyright 2018, Elsevier B.V. (G) Schematics of the actuation setup with the MAC integrated in the circular chip, placed on a supporting plate and underneath two light bulbs (Philips GreenPower LED flowering lamp deep red/white/far red to provide light for photosynthesis). The magnet is placed at a distance $r = 6.5$ mm from the rotation axis and a vertical distance $h = 2$ mm from the bottom of the ciliated surface, and the center of the ciliated area is aligned with the center of the magnet, that is $d = r = 6.5$ mm. The inside of the growth chamber is covered with aluminum foil to prevent light leakage.

and time-consuming or they disrupt the ongoing experiments.[7] Nature, after billions of years of evolution, has been an inspiration for antifouling and self-cleaning, from lotus leaves[16−19] and butterfly wings[20,21] to cilia.[22−24] Biological cilia are microhairs with a typical length between 2 and 15 μm, which are found ubiquitously in nature.[25,26] By moving in a coordinated, non-reciprocal (not time-reversible) manner, cilia have a range of different functions such as fluid pumping,[27] cell transportation,[28−30] mucus cleaning,[30,31] assisting feeding,[32−37] and self-cleaning and antifouling.[22−24] Specifically, active cilia covering the outer surfaces of mollusks and coral can generate local currents, shielding away sand and preventing settlement of a wide variety of marine fouling organisms.[22−24] Inspired by the impressive functionality of biological cilia in antifouling, researchers have been paying increasingly intensive attention to cilia. In the past decades, an increasing number of studies have been published about fabrication technologies of artificial cilia, which contributed to the development of a series of artificial cilia including electrostatic cilia,[38] magnetic artificial cilia (MAC),[39−41] optically driven cilia,[42] hydrogel-actuated cilia,[43] resonance-actuated cilia,[44] and pneumatically actuated cilia.[45] Researchers have especially used these artificial cilia as a means to transport and mix fluids.[38,41,44−52][38,41,44−52] Recently, researchers have investigated the possibility to use artificial cilia as a means to manipulate particles and create self-cleaning and antifouling surfaces, mostly using numerical computations.[53−59] Via computational and theoretical modeling, the group of Balazs and co-workers has demonstrated that both active and passive artificial cilia can be harnessed to repel microparticles in their vicinity,[57] which lays a solid foundation for subsequent experimental research on particle manipulation using artificial cilia. Using synthetic polymer particles as fouling agents, we recently demonstrated experimentally that ciliated surfaces are capable of self-cleaning because of the substantial flow generated by the cilia motion in combination with the ciliary pushing forces acting directly on the particles.[40] Another experimental study also demonstrated particle transportation by artificial cilia in air, primarily due to gravity-induced particle motion.[60] These experimental studies form the first proof-of-principle results that show the promising possibility to employ artificial cilia to create self-cleaning and antifouling surfaces. However, the artificial fouling agents used in these investigations (synthetic spherical particles) only partially mimic the real process of biofouling, a dynamic and complex process involving active fouling agents that continuously produce metabolites such as proteins. The secreted metabolites together with algae can form a conditioning layer and a "slime" film for subsequent attachment of larger and harder fouling agents. Therefore, in order to bring the concept of antifouling and self-cleaning by ciliated surfaces closer to real applications, it is of great importance to use biological fouling agents. The only previous publication on this topic known to us is a recent study of the fouling control of magnetic pillars using bacteria by Gu et al.[61]

Hence, as a crucial next step toward real-life application, in this paper, we present proof-of-principle experiments on antifouling using artificial cilia involving living biological microorganisms. Specifically, we prove that MAC can form efficient antifouling surfaces by using microalgae *Scenedesmus* sp. as fouling agents, being one of the most common biofouling agents in nature.[1,15] The particular spatial cilia arrangements investigated in this article consist of either a fully ciliated square region or a central unciliated square region surrounded by several rows of MAC. The MAC are actuated to perform a tilted conical motion at revolution frequencies between 10 and 40 Hz induced by a rotating permanent magnet. The results show that the MAC are able to prohibit microalgae to adhere to the central unciliated area after 1 week of actuation; that is,

https://dx.doi.org/10.1021/acsami.0c05403
ACS Appl. Mater. Interfaces 2020, 12, 27726−27736

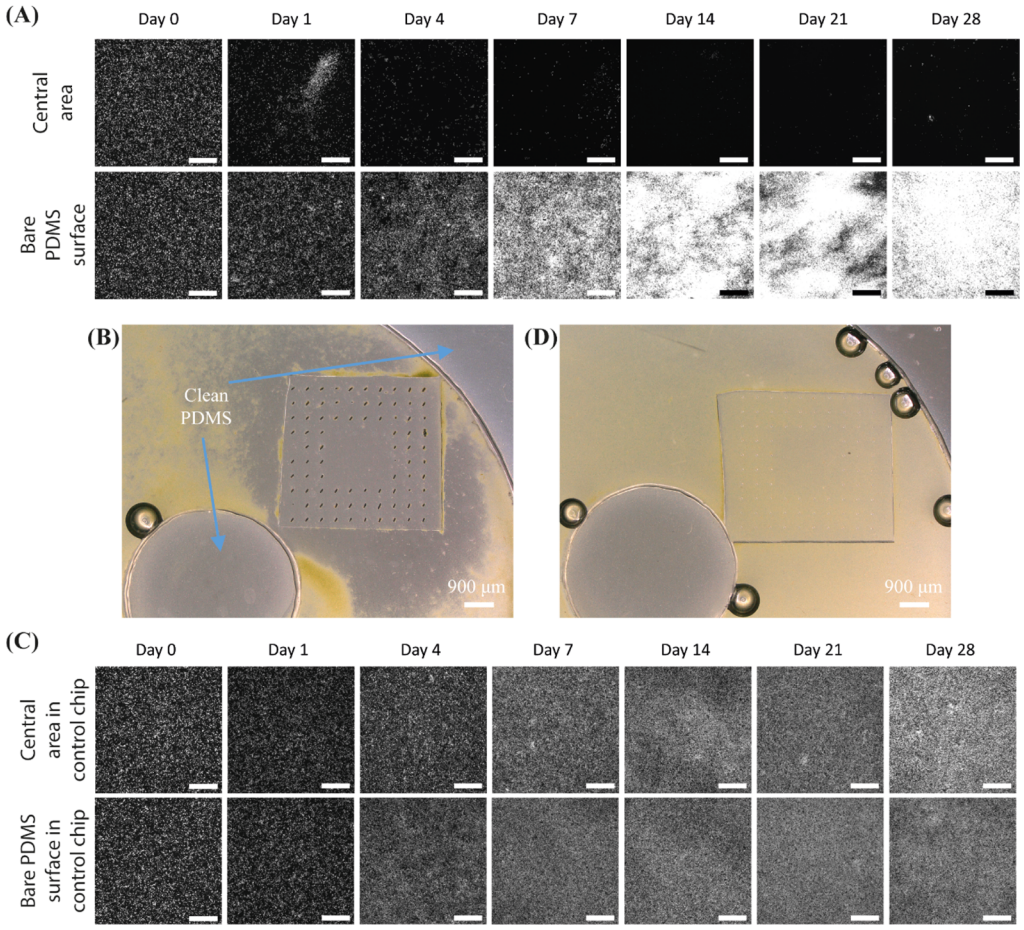

Figure 2. Microscopy images of antifouling experiments of the partially ciliated surfaces at an actuation frequency of 40 Hz. (A) Fluorescent microscopy images of one recorded representative antifouling experiment from three replicates at the observation areas indicated in Figure 1C, over a period of 28 days. The MAC have a pitch of 450 μm. All scale bars are 300 μm. In the fluorescent images, the bright dots are the algae. Note that only living algae are fluorescent and that the brightness of the algae indicates their viability, which is confirmed by the comparison between the fluorescent and bright-field images. (B) Broader bright-field microscopy image of the ciliated part after 28 days of actuation of one representative experiment from three replicates, showing that the central unciliated area is almost perfectly clean, from a comparison with the clean part of the PDMS chip. In the bright-field images, the green dots are the algae, and the color of clean PDMS is grey. The circle with a black edge and a bright center is an air bubble. (C) Fluorescent microscopy images of one recorded representative control experiment from three replicates at the observation areas indicated in Figure 1C, over a period of 28 days. (D) Broader bright-field microscopy image of a representative control experiment from three replicates after 28 days, showing that the complete channel, including the central area surrounded by non-moving cilia, is fouled indiscriminately.

the MAC are capable of antifouling. Moreover, even after 1 week of colonization by the microalgae (before activation of the MAC), the MAC can still clean the central unciliated surface within 2 weeks of actuation; that is, the MAC are capable of self-cleaning. We expect that the prevention of the microalgae attachment will deter the establishment of the subsequent "soft" and "hard" macrofouling. Our findings offer insights to develop novel types of antifouling and self-cleaning surfaces for a variety of practical applications, such as lab-on-a-chip devices and water quality analyzers.

2. RESULTS AND DISCUSSION

2.1. Ciliated Surface and Experimental Setup. Figure 1A shows that the polydimethylsiloxane (PDMS)-based MAC used in this article have a cylindrical shape with a diameter of 50 μm and a height of 350 μm. The MAC were fabricated using a facile and reproducible micromolding method (see the Supporting Information).[41] Initially, experiments were performed using "fully ciliated surfaces" that were covered with the MAC arranged in a staggered configuration with a pitch of 450 μm (Figure S3A). The results showed a strong antibiofouling effect (see the Supporting Information for details). However, it is more desirable to have a completely clear area for devices that include a sensor area (such as an optical sensor) where anything covering the sensor surface may disrupt the sensing. To account for this, ciliated surfaces were created that consist of a central unciliated square region surrounded by three rows of MAC on each side (Figure 1B), which are termed "partially ciliated surfaces". The sensor could be located in the central unciliated region. Here, in the main text, we show detailed experimental results of the partially ciliated surfaces (for the fully ciliated surfaces, the reader is referred to the Supporting Information).

The amount of "absent" cilia is $4 \times 4 = 16$ in a full array of 10×10, so there are 84 cilia in total. The pitch of the MAC was varied between 250, 350, and 450 μm, which corresponds to a central unciliated area of 1.44, 2.89, and 4.84 mm^2, respectively.

https://dx.doi.org/10.1021/acsami.0c05403
ACS Appl. Mater. Interfaces 2020, 12, 27726−27736

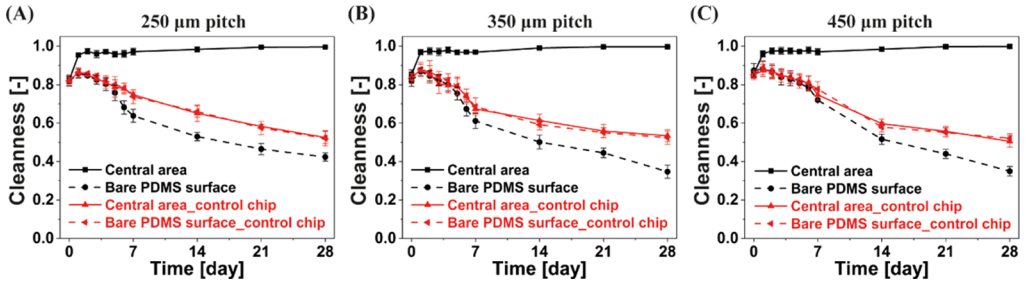

Figure 3. Calculated antifouling capability over time for the partially ciliated surfaces covered with MAC with a pitch of (A) 250 μm, (B) 350 μm, and (C) 450 μm. The revolution frequency of the MAC is 40 Hz. If the *Cleanness* equals 1, no algae are present in the observed area; if it equals 0, the whole area is completely polluted. The error bars are the standard deviations of three identical but independent experiments.

The ciliated surface was integrated in a closed circular microfluidic chip with a rectangular cross section with a channel width of 7.5 mm and a channel height of 2 mm (Figure 1C). The chip was filled with the algae *Scenedesmus* sp. (Figure 1D) suspended in the culture medium (concentration: 1×10^4 cells μL^{-1}), see the Experimental Section for details on the algae culture. The algae have a crescent shape with an average length of 12 μm and an average width of 4.6 μm. The MAC were actuated to perform a tilted conical motion (Figure 1E,F) by a homebuilt magnetic setup (Figure 1G, see the Experimental Section for details) at a constant revolution frequency. This motion cycle contains an "effective stroke" when the cilium moves mostly perpendicular to the surface and a "recovery stroke" when the cilium is moving close to the substrate, which was demonstrated to be a simple yet effective asymmetric nonreciprocal motion to generate net fluid flows.[62] Indeed, we demonstrated that with such a motion, the molded MAC were capable of generating substantial versatile flows in a microfluidic chip,[41] which can induce hydrodynamic shear forces on surrounding particles.

2.2. Antifouling Capability of the Ciliated Surfaces. Experiments to study the antifouling properties of the partially ciliated surfaces were done by actuating the MAC immediately after filling the microfluidic chip with the microalgae (see the Experimental Section for details). Control experiments were performed simultaneously under exactly the same conditions by simply replacing the MAC with nonmagnetic PDMS pillars of the same geometry so that there is no flow in the control chips.

Figure 2 shows the fluorescent microscopy images of one recorded experiment and a control experiment over a period of 4 weeks (see Figure S4 for the corresponding bright-field images). Note that only the living algae are fluorescent and that the brightness of the algae indicates their viability, which is confirmed by a comparison between the fluorescent and bright-field images. The MAC have a pitch of 450 μm, and they perform the tilted conical motion at 40 Hz. As shown in Figure 2A, in the chip integrated with the MAC, initially the algae cover the substrate of the ciliated chip uniformly and no large clusters of algae are visible, and subsequently they are gradually removed from the central unciliated area. The central area is almost completely clean after 1 week of actuation, and it stays clean for another 3 weeks. Note that the experiment was stopped after a period of 4 weeks, but we expect that the central unciliated surface will remain clean if the experiment is continued. It also important to note that the operation duration to maintain a clean surface could be reduced through actuating the cilia from the start, before the fouling begins, in order to prevent the entrance of the algae into the ciliated surface, which is inspired by the "particle exclusion" results reported in our earlier work.[40]

In contrast, the algae do attach to the bare PDMS surface in the same chip (in the observation area opposite to the ciliated area, indicated in Figure 1C), and grow healthily within the first week. After 2 weeks, the observed color and morphology of the algae slightly change which is probably due to the growth medium and CO_2 level not being sufficient for the prolonged wellbeing of the algae. The algae do stay alive though during the whole period of the experiment. Figure 2B shows a wider bright-field microscopy image of the experiment, indicating that after 28 days of actuation the central unciliated area is almost perfectly clean (from a comparison with the clean central circular part of the PDMS chip, which is not in contact with the fluid). Most of the rest of the channel, however, is fouled by the algae. As shown in Figure 2C, in the control chip integrated with the passive PDMS pillars, the algae do attach to the bare central area and the bare PDMS surface indiscriminatingly, and they grow and colonize the surface gradually, creating a fouling film. Figure 2D shows a wider bright-field microscopy image of the control experiment, showing that the passive pillars have no influence on the colonization by algae. Note that we did observe almost no algae adhering to the body surface of the cilia as shown in Figure S5.

The antifouling capacity was quantified using an in-house developed image processing algorithm (see the Experimental Section), which uses both the bright-field and the fluorescent images. The calculated *Cleanness* is plotted in Figure 3 for MAC with different pitches at a constant revolution frequency of 40 Hz. When *Cleanness* equals 1, all algae are removed from the analyzed area, that is the area is completely clean; when *Cleanness* is 0, the whole area is completely polluted. It is clear that the MAC are able to clean the central unciliated area within 1 week and can maintain the cleanness of this area in the following weeks, preventing colonization of the algae, for MAC with all different pitches and for a central unciliated area as large as 4.84 mm^2, which is comparable to the size of typical sensors used in microfluidic devices such as the antibody-based sensor introduced by Bruls et al.[63] and the electrochemical sensor reported by Nie et al.[64] The latter is limited only by our design and can potentially be extended by fabricating MAC with a pitch larger than 450 μm or fabricating partially ciliated surfaces with more cilia "absent". Moreover, when an even larger clean surface is necessary and when the surface allows the presence of the artificial cilia, the large cleaning surface can be accomplished using the fully ciliated surfaces as demonstrated in the Supporting Information. In contrast, the bare PDMS surface in the same chip and the observation areas

https://dx.doi.org/10.1021/acsami.0c05403
ACS Appl. Mater. Interfaces 2020, 12, 27726−27736

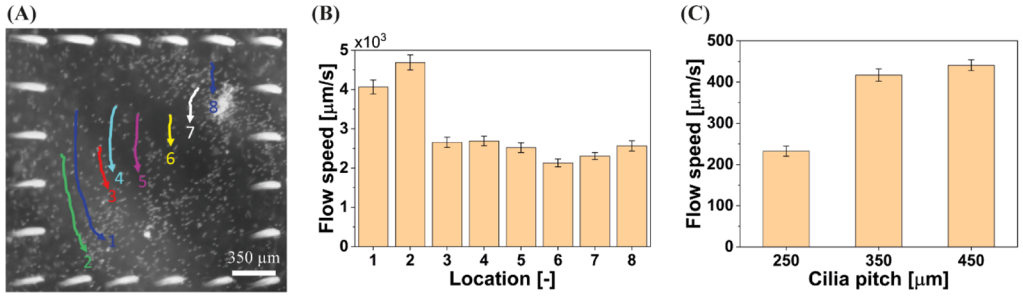

Figure 4. Fluid flow generated by the MAC at 40 Hz. (A) Snapshot of one experiment to measure the flow generated by the MAC with a pitch of 350 μm in the central unciliated area. The colored lines (1−8) indicate the trajectories of the traced particles at different locations (and tracked for different durations) in the horizontal plane; they are moving on the PDMS substrate surface, that is the vertical distance between the center of the traced particles and the PDMS substrate equals the radius of these particles (6 μm). The white dots are 12 μm tracing particles. See also the Supporting Information, Movie S1. (B) Measured local flow speed calculated from tracer particle trajectories at the locations indicated in panel A. The MAC have a pitch of 350 μm. (C) Measured global flow speed in the channel integrated with ciliated surfaces with a cilia pitch of 250, 350, and 450 μm, respectively; see also the Supporting Information, Movie S3. The error bars are the standard deviations of the measurements.

in the control chip are increasingly fouled over the recorded period, which indicates that the algae do stay alive. Figure 3 also shows that the final status of the bare PDMS surface in the ciliated chip is worse than the surface in the control chip, which is probably because (1) the algae expelled from the central unciliated area accumulate on the bare PDMS surface and (2) the algae grow faster in the ciliated chip because the cilia-motion-generated flow enables the algae to get better access to the nutrients in the medium. Note that the *Cleanness* initially increases (at day 1) for the bare PDMS surface in the ciliated chip as well as for the observation areas in the control chip, suggesting an initial decrease in algae, which can be seen from the fluorescent images; this is probably the result of some algae not surviving immediately after injecting into the chips because they have not adapted to the closed chip environment yet. However, subsequently, the algae do continuously grow in these experiments after day 1.

There are two predominant mechanisms underlying the antifouling effect. First, the MAC motion induces substantial flow within the central unciliated area (see the Supporting Information, Movie S1). The measured flow generated by MAC with a pitch of 350 μm, calculated from trajectories of tracer particles moving over the PDMS substrate surface, at the locations indicated in Figure 4A, is plotted in Figure 4B. The flow speed close to the PDMS substrate surface is approximately 3×10^3 μm s^{-1}, which can induce strong shear stress and corresponding shear forces (around 0.4 Pa and 30 pN, respectively, see the Supporting Information for details of the calculation) on the algae lying on the PDMS substrate. The strong forces overcome the adhesive strength between the algae and the PDMS surface, which results in the algae being swept away and lifted up from the substrate. In addition, the liquid within the central area is continuously flushed out of this area, as seen in the Supporting Information, Movie S2, which results in the lifted algae being expelled from the central area. Second, as shown in Figure 4C, the MAC motion can generate substantial global flow (with speeds on the order of 10^2 μm s^{-1}) in the channel (see also the Supporting Information, Movie S3), which carries away the algae from the ciliated area along the direction of the effective stroke of the MAC. As the algae have a larger density than the medium, they gradually settle when flowing downstream. Moreover, the maximal global flow speed is approximately 1 order of magnitude smaller than the flow speed within the central area, which is probably not sufficient to flush away the algae lying on the PDMS substrate. As a result, the algae accumulate downstream from the ciliated area as shown in Figure 2A (bare PDMS surface).

It is meaningful to argue here that the antifouling effect of the strong local shear flow induced by the MAC has advantages for the use of conventional flow generation methods. First, the high local velocity near the surface that induces a relatively high shear stress (0.4 Pa) on the algae is mostly not reached in microfluidic flows driven by, for example, a conventional syringe pump, where wall shear stresses typically are 1 order of magnitude smaller (details are available in the Supporting Information). Second, even if it would be possible to reach the high shear stresses in microfluidic devices using a conventional pumping method, this is often not desirable because it may interfere with the primary function of the device. For example, in biorelated lab-on-chip applications, flow can have a profound impact on the status of cells and tissues, and applying a global flow in the system for the purpose of antifouling during operation using conventional pumps may cause unwanted side effects. A localized, independent targeted cleaning means (e.g., for creating a clean optical or biochemical sensing area) using artificial cilia will minimize such effects on the overall system. Third, for field applications in natural waters (such as, submerged sensors), external flow is either not present or it is uncontrolled, and our artificial cilia provide a solution to create a controlled local antifouling flow, which is hard to achieve using conventional means. Finally, our artificial cilia method does not use up any additional pumping fluid, whereas a conventional source such as a syringe pump continuously pumps samples and reagents into the perfused channels and reaction chambers, which uses a large amount of samples and results in increased cost.

We performed antifouling experiments using different actuation frequencies (i.e., 10, 20, 30, and 40 Hz) to further verify the claim that the generated hydrodynamic shear forces are key for effective antifouling. Note that these experiments were performed exactly the same as the aforementioned antifouling experiments, except for the variation of the actuation frequency. The results are shown in Figure 5. It is clear that the cleanness is better at a higher actuation frequency after a specific actuation duration. This trend is similar to that reported in our previous study on particle removal.[40] It has been reported that the generated fluid flow is higher at a higher actuation frequency,[41] which implies that a higher hydrodynamic shear force is exerted on the algae at a higher actuation frequency. Therefore, this group of experiments

https://dx.doi.org/10.1021/acsami.0c05403
ACS Appl. Mater. Interfaces 2020, 12, 27726−27736

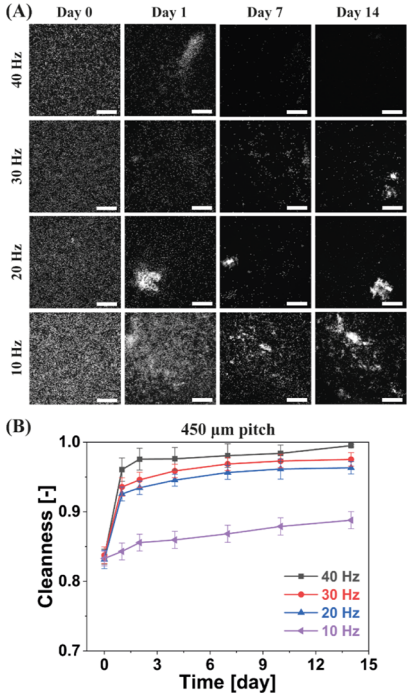

Figure 5. Impact of the actuation frequency on the antifouling capability of the MAC. (A) Fluorescent microscopy images of one group of recorded representative antifouling experiments from three replicates at the "central" observation area indicated in Figure 1C, over a period of 14 days. The MAC have a pitch of 450 μm. All scale bars are 300 μm. In the fluorescent images, the bright dots are the algae. (B) Calculated antifouling capability over time for partially ciliated surfaces at different actuation frequencies. If the *Cleanness* equals 1, no algae are present in the observed area. The error bars are the standard deviations of three identical but independent experiments.

strongly indicates that the hydrodynamic shear forces applied on the algae are indeed the key to the antifouling, and that sufficient actuation frequency is needed in order to remove the fouling agents in order to overcome their specific adhesion strength to the surface.

Knowing the adhesion forces between the algae and the PDMS substrate may provide further insights into the antifouling mechanism. However, different adhesion characterization methods that have been attempted by others give dramatically different results.[65] In addition, knowing them in detail does not add substantially to the main message of this article. Therefore, characterization of the adhesion forces is beyond the scope of the current article.

The antifouling capability of artificial cilia will probably deter the establishment of the "slime" film in real devices and thus inhibit fouling by macrofouling agents;[1−6] this will be a subject of future research.

2.3. Self-Cleaning Capability of the Ciliated Surfaces.

Self-cleaning experiments were done by starting the actuation of the MAC 1 week after filling the microfluidic chip with microalgae (see the Experimental Section for details). During this week, the algae were left growing under static conditions, which offers enough time for the algae to colonize the surface, and this period of time is termed the "culturing period". Control experiments were performed simultaneously under exactly the same conditions by simply replacing the MAC with nonmagnetic PDMS pillars of the same geometry. The main purpose of this type of experiments is to demonstrate experimentally that the MAC are able to remove the algae from the central unciliated area even when the algae settle or attach to the surface.

Figure 6 shows the fluorescent microscopy images of one recorded experiment over a period of 3 weeks (see Figure S6 for the corresponding bright-field images). The MAC have a pitch of 450 μm. As shown in Figure 6A, during the culturing period, the algae cover the bottom of the chip uniformly and grow healthily. Subsequently, when the MAC are actuated to perform the tilted conical motion (which is termed "cleaning period"), the algae are gradually removed from the central unciliated area. The central area is almost completely clean after 2 weeks of actuation. In contrast, the algae remain attached to the bare PDMS surface in the same chip and grow healthily. These experiments raise a question: how many days (y) should the MAC be actuated to clean a surface that has been contaminated for a number of weeks (x). This would give a quantitative performance readout of the MAC, which is a subject of future work.

The self-cleaning capacity was quantified using the in-house developed image processing algorithm (see the Experimental Section). The calculated *Cleanness* is plotted in Figure 6B−D for MAC with different pitches. Obviously, the algae grow and colonize the surface during the culturing period, and they are gradually expelled from the central unciliated area within the first week of the cleaning period, and over 99% of the algae are washed away after 1 week of cleaning for MAC with all different pitches, even for a central unciliated area as large as 4.84 mm^2. In contrast, the algae progressively continue to colonize the bare PDMS surface and the control chip. Notably, for antifouling experiments reported in Figure 3, it takes only 2 days to reach a *Cleanness* of 99%, whereas for self-cleaning experiments of Figure 6, it is approximately 1 week, which indicates that the algae do colonize and adhere to the surface during the culturing period. This clearly indicates that the ciliated surfaces can not only prevent algae from settling, but also clean away the algae that have already settled, most likely because of the generated hydrodynamic shear forces explained above.

As our MAC turned out to be capable of self-cleaning, we hypothesized that when the MAC are actuated periodically, for example, actuated for 16 h and in rest for 8 h during a day, the central unciliated area can still be cleaned. This periodical actuation mode would be meaningful for applications that need to run in intervals and/or are incompatible with MAC actuation. To verify this hypothesis, we carried out experiments in which the cilia were actuated for 16 h and subsequently kept statically for 8 h within 1 day. The results are depicted in Figure S7, which shows that the periodical actuation also results in self-cleaning, although a longer cleaning time is required compared to the continuous actuation mode.

3. CONCLUSIONS AND OUTLOOK

We have demonstrated the antifouling and self-cleaning capabilities of MAC with real biological fouling agents—microalgae, which are one type of common fouling agents found in nature. We have shown this for ciliated surfaces with a bare unciliated central region (allowing to locate an optical sensor, for instance) surrounded with rows of MAC, termed the "partially ciliated surface". It was found that the MAC are very efficient in repelling algae from the central unciliated area of at least 4.84 mm^2. This efficiency was demonstrated for two

https://dx.doi.org/10.1021/acsami.0c05403
ACS Appl. Mater. Interfaces 2020, 12, 27726−27736

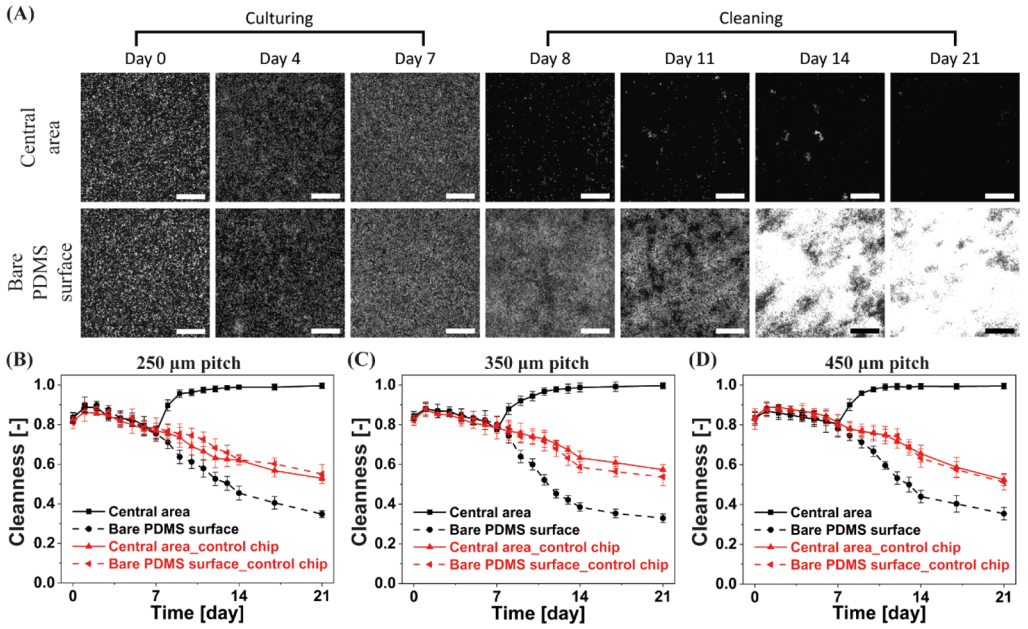

Figure 6. Self-cleaning capability of the partially ciliated surfaces. (A) Fluorescent microscopy images of one recorded representative self-cleaning experiment from three replicates at the observation areas indicated in Figure 1C, over a period of 21 days. The MAC have a pitch of 450 μm. All scale bars are 300 μm. In the fluorescent images, the bright dots are the algae. (B–D) Calculated self-cleaning capability over time for partially ciliated surfaces covered with MAC with a pitch of (B) 250, (C) 350, and (D) 450 μm. The first 7 days form the culturing period, and subsequent 2 weeks form the cleaning period. If the *Cleanness* equals 1, no algae are present in the observed area; if it equals 0, the whole area is completely polluted. The error bars are the standard deviations of three identical but independent experiments.

scenarios: (1) actuating the cilia immediately after injecting the algae into the chip, showing "antifouling" and (2) starting to actuate the cilia 1 week after injecting the algae into the chip and leaving them to grow and colonize the surface under static conditions, showing "self-cleaning". We showed that both the local and global flow generated in the central unciliated area by the actuated MAC are substantial, resulting in hydrodynamic shear forces acting on the algae, which are most likely the key hydrodynamic mechanism underlying the efficient antifouling and self-cleaning. The latter is supported by the clear dependency of the antifouling on the actuation frequency, strongly indicating that fouling agents are more effectively removed if the hydrodynamic shear forces are sufficient to overcome the specific adhesion strength of the fouling agents to the surface. The prevention of the microalgae attachment is expected to deter the subsequent establishment of the "soft" and "hard" macrofouling in real applications. These findings and insights contribute to a further step to the development of a novel type of antifouling and self-cleaning surface that can be relevant for a variety of industries and applications, including marine sensors, water quality analyzers, and lab-on-a-chip devices. Note that the applicability of our technique is not only limited to using a rotating magnet to actuate the cilia. Electrostatic fields,[38] electromagnetic fields,[66,67] resonance,[44] pneumatic pressure,[45] and even ambient flow[54,58] can also serve as alternatives for generating artificial ciliary motion. It is also important to stress that we did not observe any rupture or break of the MAC or the reduction of the cilia motion during the period of the long-run experiments (Figure S5), which shows that our MAC are mechanically robust.

Our results provide a first experimental proof-of-principle of the antifouling and self-cleaning capabilities of artificial cilia using real biological fouling agents. Because of the limited scope of the experiments, this work is merely a first small step in this direction and broad conclusions about the prevention of biofouling cannot be drawn. We used only one type of material (PDMS, the most common one in microfluidics) and one type of biofouling agent (microalgae *Scenedesmus* sp., one of the most common biofouling agents in nature), and we only studied the effect of a limited number of parameters including different types of ciliated surfaces (fully ciliated and partially ciliated surfaces), different pitches, different frequencies, and algae colonization before the actuation of the artificial cilia. Also, our analysis was based on two-dimensional microscopy images and therefore it does not explicitly account for the three-dimensional (3D) nature of the biofilms, and we did not perform any biological analysis. Such controlled work is a prerequisite to more extensive experiments, and for the final implementation into real applications, more fundamental and applied research and technological development is required. One topic of future research could be the use of other biofouling agents than microalgae *Scenedesmus* sp. to study the two subsequent stages of biofouling, that is, the accumulation of soft (stage 3) and hard (stage 4) phases.[1−6] Also, other types of substrate materials could have an effect, especially in self-cleaning. In addition, testing in practically relevant circumstances (e.g., at different temperatures or in fluids with varying salinity), on real devices, and during field tests in natural waters should be subjects of future research. In the analysis, biological techniques such as biomass determination and 3D fluorescence imaging should be included like is done in biofilm research. Finally, fundamental studies of biological aspects, for example, the analysis of algal physiology, metabolic activity, 3D biofilm structure, and biomass and research on the effectiveness of the ciliated surfaces against biofilm matrix formation, could provide basic knowledge of the anti-fouling and self-cleaning process that can be helpful in future design of optimized methods.

https://dx.doi.org/10.1021/acsami.0c05403
ACS Appl. Mater. Interfaces 2020, 12, 27726−27736

4. EXPERIMENTAL SECTION

4.1. Microalgae. Microalgae *Scenedesmus* sp. (Culture Collection of Algae and Protozoa, SAMS Limited, Scottish Marine Institute) were cultured in a culture medium (modified BB medium with vitamins (3N-BBM + V, see https://www.ccap.ac.uk/media/documents/3N_BBM_V.pdf for details) in a home-built growth chamber (Figure S1A) consisting of (i) a PMMA box covered inside with aluminum foil to prevent light leakage, (ii) Duran Erlenmeyer narrow-neck flasks containing the algae and culture medium, (iii) a shaker running at 100 rpm to prevent algae from settling, (iv) two light bulbs (Philips GreenPower LED flowering lamp deep red/white/far red) to provide light for photosynthesis, and (v) a thermometer to measure the temperature in the growth chamber. A commercial aquarium pump (Superfish 4 outlets, output 2.5 × 4 L min^{-1}) was connected to the flasks by silicon tubes and a sterile syringe filter (Minisart NML, pore size 0.2 μm), bubbling air to support photosynthesis into the medium and to facilitate suspension of the algae. All flasks, tubes, silicon stoppers, and medium were sterilized in an autoclave at 120 °C before each experiment. All cell transfer and handling were done within a sterile laminar flow hood. The light provided by the two bulbs was monitored at 4000 lux with a light−dark cycle of 16−8 h. The temperature in the growth chamber was regulated at 28 °C when the light was on and at 22 °C with the light off. Cells were counted as a function of culture time with a hemocytometer (Thoma, Paul Marienfeld GmbH & Co. KG), the results of which are shown in Figure S1B. Initial cell culture was performed for five different strains of microalgae, before selecting *Scenedesmus* sp. as the strain of choice for the experiments reported in this paper, as explained in the Supporting Information.

4.2. Magnetic Actuation Setup. The homebuilt magnetic actuation setup (shown in Figure 1G) was composed of a manual linear XYZ translational stage at the bottom, an electric motor in the middle, an magnet mounted off-axis on the motor, and a safety box containing the supporting plane on top of which the chip containing the MAC could be placed. The magnet, which had a geometry of 20 × 20 × 10 mm^3 with a remnant flux density of 1.3 T, was positioned at an offset of r = 6.5 mm with respect to its rotation axis. The center of the ciliated surface was vertically aligned with the center of the magnet (when the magnet is in its rightmost position as in Figure 1G), that is, $d = r$ = 6.5 mm. The supporting plane was a transparent glass plate of thickness of 1.5 mm, coated with a layer of PDMS (100 μm, base to curing agent weight ratio = 10:1, cured at 80 °C for 3 h). A high-speed camera (Phantom V9) mounted on a stereo microscope (Olympus SZ61) was used to capture the movement of the MAC from above right by taking image sequences at a frame rate of 1000 fps.

4.3. Characterization of the Flow Generated by the MAC. The flow was characterized at specific flow observation areas, indicated in Figure 1C. The liquid we used was deionized water, and the flow speeds were visualized by seeding the fluid with 12 μm polystyrene tracer particles (micromod Partikeltechnologie GmbH). A high-speed camera (Phantom V9) connected to a stereo microscope (Olympus SZ61) was used to record the movement of the tracer particles by taking image sequences at a specific frame rate of 100 fps for the central area in the ciliated region, and 10 fps for the bare PDMS area. The speed of the tracer particles on the PDMS substrate surface in the central area surrounded by the MAC and in the geometrical center of the microfluidic channel in the bare PDMS area (i.e., at a height of 1 mm above the channel substrate, where the flow speeds are the highest) was measured by the Manual Tracking analysis using ImageJ.

4.4. Experimental Process of Antifouling and Self-Cleaning Experiments. Before starting a new experiment, the microfluidic chip, the supporting glass plate, and a syringe with a needle were sterilized with 70% ethanol and UV light. After sterilization, the medium containing the algae with a density of 1 × 10^4 cells μL^{-1} was injected with the sterilized syringe into the sterilized chip under a sterile laminar flow hood. Then the sample was transferred to the actuation setup (Figure 1G). In the "antifouling" experiments, the MAC were immediately actuated to perform the tilted conical motion as shown in Figure 1E,F. Light was provided by two light bulbs (Philips GreenPower LED flowering lamp deep red/white/far red) with a light−dark cycle of 12−12 h and a light intensity of 9000 lux, so that the algae could perform photosynthesis. The temperature in the growth chamber as shown in Figure 1G was regulated at 28 °C when the light was on and at 22 °C with the light off. Another chip containing pure (nonmagnetic) PDMS pillars with the same dimension as the MAC was placed near the chip containing the MAC, as a control experiment. Because PDMS is gas permeable, the medium did evaporate during the experiments and bubbles were generated from both medium evaporation and photosynthesis of the algae. To ensure that there was enough culturing medium in the chip, the medium was carefully added every 2 days into the chip to remove all of the bubbles (no algae were flushed out of the chip) under a sterile laminar flow hood. Each type of experiment was performed at least three times in the same way. A microscope (Keyence VHX-5000 Digital Microscope) was used to take bright-field images of the observation areas as indicated in Figure 1C. The living algae are fluorescent and therefore they can be observed and analyzed clearly using fluorescent microscopy. A camera (Leica DFC9000 GT) mounted on another microscope (Leica DM4000 M) was used to capture fluorescent images of the observation areas. The used filter cube was LEICA I3 (11513878 BZ: 01), which is composed of a bandpass excitation filter (450−490 nm), a dichromatic mirror (510 nm), and a longpass suppression filter (515 nm). Note that from the comparison between the fluorescent and bright-field images, we could confirm that only living algae are fluorescent and that the brightness of the algae indicates their viability. We took two types of microscopy images in order to increase the reliability of our analysis method because the bright-field images can capture both live and dead algae, whereas the fluorescent images can only capture the live algae.

The only difference between the "self-cleaning" experiments and the antifouling experiments was that in the self-cleaning experiments, the actuation of the MAC was started 1 week after the microfluidic chip was injected with the algae and placed in the actuation setup, to leave the algae growing under static conditions, rather than immediately after placing the chip in the growth chamber. During the first week of static growth, the algae were subject to the same light and temperature conditions as those during the actuation of MAC, and the medium in the chip was refreshed every 2 days as described above.

4.5. Method to Quantify the Antifouling and Self-Cleaning Capacities. The obtained bright-field microscopy images were quantitatively analyzed in the following way. First, the RGB values of each pixel of the experimental images were extracted and analyzed using an in-house developed algorithm. Subsequently, through a systematic exploration of the most distinguishing image features, we found that the key to identifying the degree of pollution was the ratio between the G value and the B value, as the R value barely varied for all polluted situations of different levels. Then, the pollution condition of the observed areas was classified into three levels as shown in Table 1: unpolluted, normally polluted, and heavily polluted. We defined the pollution condition in this way because the processed images generated with the indicated data matched best with the original experimental images (see Figure S8). The generation of the images was done in the following way. The unpolluted area was colored white with the RGB values of (255, 255, 255); the normally polluted area was colored greenish with the RGB values of (100, 200, 100); and the

Table 1. Definition of the Pollution Condition of the Observed Areas

	bright-field images	fluorescent images
pollution condition	ratio between G value to B value	range of pixel values
unpolluted	[0, 1.15)	[0, 12,000)
normally polluted	[1.15, 1.6)	[12,000, 45,000)
heavily polluted	[1.6,∞)	[45,000, 65,536]

https://dx.doi.org/10.1021/acsami.0c05403
ACS Appl. Mater. Interfaces 2020, 12, 27726−27736

Table 2. Percentage of Polluted Areas (as Defined in Table 1) Relative to the Total Analyzed Area, Determined from the Images in the Supporting Information

time			day 0 (%)	day 1 (%)	day 4 (%)	day 7 (%)	day 14 (%)
central area	normally polluted	bright-field images	43.16	10.24	2.84	1.1	1.02
		fluorescent images	35	5.33	1.02	0.51	0.3
		difference	8.16	4.91	1.82	0.59	0.72
	heavily polluted	bright-field images	0.3	0.15	0.01	0	0
		fluorescent images	0.35	0.09	0.04	0.07	0.01
		difference	0.05	0.06	0.03	0.07	0.01
bare PDMS surface	normally polluted	bright-field images	37.45	50.49	87.64	74.06	54.71
		fluorescent images	35.42	47.42	83.98	73.22	50.73
		difference	2.03	3.07	3.66	0.84	3.98
	heavily polluted	bright-field images	0.13	0.73	3.47	21.53	44.95
		fluorescent images	0.18	0.62	5.37	25.33	49.26
		difference	0.05	0.11	1.9	3.8	4.31

heavily polluted area was colored completely green with the RGB values of (0, 255, 0). Afterward, the antifouling/self-cleaning capacities were quantified as

$$\text{Cleanness} = 1 - \frac{A_{\text{heavily}} + \frac{1}{2}A_{\text{normally}}}{A_{\text{total}}}$$

where A_{total} is the total observation area, A_{heavily} is the area of the heavily polluted surface, and A_{normally} is the area of the normally polluted surface. As a result, the range of *Cleanness* is [0, 1]. *Cleanness* = 1 means there are no algae at all within the observation area, that is, the whole observation area is completely clean; *Cleanness* = 0 means that the whole observation area is heavily polluted. Finally, substitution of the pixel numbers of the three kinds of areas into the formula resulted in a quantitative measure of the antifouling/self-cleaning capabilities of an experiment.

The fluorescent images were quantified in the following way. First, the pixel values (representing the brightness or intensity) of the fluorescent images were extracted using the imread function in MATLAB. Subsequently, by comparing the fluorescent images with the bright-field images, it was concluded that a higher pixel value means that this pixel is more heavily polluted. Therefore, the pixel values can be used to distinguish unpolluted, normally polluted, and heavily polluted areas. Note that the obtained fluorescent images are flood fill images, which have pixel values ranging from 0 to 65,536. This range is much larger than the RGB value range of the bright-field images, which contributes to a much higher precision in distinguishing the pollution condition. Then, the pollution condition was defined as summarized in Table 1. Afterward, the antifouling/self-cleaning capabilities were quantified using the same equation as for the bright-field images (see above). Finally, by substituting the pixel numbers into the formula, we obtained the antifouling/self-cleaning capabilities of an experiment. The obtained data were plotted into figures. Each data point was obtained by averaging the results of both the bright-field and fluorescent images of at least three identically but separately performed experiments. The Supporting Information contains the MATLAB codes used and includes images to demonstrate how the codes work.

In further analysis, we counted the algae left in the central unciliated area of both the bright-field and fluorescent images shown in the Supporting Information using ImageJ, and the difference between the number of algae in the two types of images was found to be within 5%. This shows that most algae still left on the surface after cleaning (although there may be little) are alive. Moreover, we measured the percentage of the "normally polluted area" and the "heavily polluted area" (as defined according to Table 1) of both types of images in the Supporting Information using the in-house algorithm, and the results (see Table 2) show that the difference between the two types of images is also within 5%, except for one case on day 0 (where apparently some more dead algae were present). These measurements again show that, in almost all our measurements, almost all algae are alive and that the cilia can remove almost all algae independent of whether they are alive or not.

■ ASSOCIATED CONTENT

Supporting Information

The Supporting Information is available free of charge at https://pubs.acs.org/doi/10.1021/acsami.0c05403.

Algae culturing—different algae strains; fabrication process of MAC; antifouling experiments of fully ciliated surfaces; bright-field microscopy images of antifouling and self-cleaning experiments; calculation of the hydrodynamic shear force acting on the algae; self-cleaning efficiency of partially-ciliated surfaces; and verification of the image processing method (PDF)

High-speed video showing the cilia-motion-generated flow on the PDMS substrate surface in the central unciliated area as shown in Figure 1C (MP4)

High-speed video showing the flow generated by the MAC both in and out of the ciliated area (MP4)

High-speed video showing the cilia-motion-generated global flow in the bare PDMS area as shown in Figure 1C (MP4)

In-house developed algorithms used in this article to quantitatively analyze the obtained microscopy images (ZIP)

■ AUTHOR INFORMATION

Corresponding Author

Jaap M. J. den Toonder − *Department of Mechanical Engineering and Institute for Complex Molecular Systems, Eindhoven University of Technology, 5600 MB Eindhoven, The Netherlands*; Email: J.M.J.d.Toonder@tue.nl

Authors

Shuaizhong Zhang − *Department of Mechanical Engineering and Institute for Complex Molecular Systems, Eindhoven University of Technology, 5600 MB Eindhoven, The Netherlands*; orcid.org/0000-0002-4103-1474

Pan Zuo − *Department of Mechanical Engineering, Eindhoven University of Technology, 5600 MB Eindhoven, The Netherlands*

Ye Wang − *Department of Mechanical Engineering and Institute for Complex Molecular Systems, Eindhoven University of Technology, 5600 MB Eindhoven, The Netherlands*

Patrick Onck − *Zernike Institute for Advanced Materials, University of Groningen, 9712 CP Groningen, The Netherlands*

https://dx.doi.org/10.1021/acsami.0c05403
ACS Appl. Mater. Interfaces 2020, 12, 27726−27736

Complete contact information is available at:
https://pubs.acs.org/10.1021/acsami.0c05403

Author Contributions

S.Z. and J.M.J.d.T. designed the research; S.Z. performed research and collected data; S.Z. and P.Z. analyzed the data; S.Z. wrote the manuscript; P.Z., Y.W., P.O., and J.M.J.d.T. revised the manuscript.

Notes

The authors declare no competing financial interest.

■ ACKNOWLEDGMENTS

S.Z. is financially supported by the China Scholarship Council under grant no. 201506030055. The research leading to these results has also received funding from the European Research Council (ERC) under the European Union's Horizon 2020 research and innovation programme under grant agreement no. 833214. We would like to thank Lucien Cleven, Erwin Dekkers, and Edwin Suijkerbuijk for constructing the magnetic actuation setup, Dr. Allison Schaap and Junyi Yao for the useful suggestions on culturing algae, and Dr. Mark van Turnhout for helping in taking phase-contrast microscopy images of the algae.

■ REFERENCES

(1) Kirschner, C. M.; Brennan, A. B. Bio-Inspired Antifouling Strategies. *Annu. Rev. Mater. Res.* **2012**, *42*, 211−229.
(2) Chambers, L. D.; Stokes, K. R.; Walsh, F. C.; Wood, R. J. K. Modern Approaches to Marine Antifouling Coatings. *Surf. Coat. Technol.* **2006**, *201*, 3642−3652.
(3) Callow, M. E.; Callow, J. A.; Pickett-Heaps, J. D.; Wetherbee, R. Primary Adhesion of Enteromorpha (Chlorophyta, Ulvales) Propagules: Quantitative Settlement Studies and Video Microscopy. *J. Phycol.* **1997**, *33*, 938−947.
(4) Abarzua, S.; Jakubowski, S. Biotechnological Investigation for the Prevention of Biofouling. 1. Biological and Biochemical Principles for the Prevention of Biofouling. *Mar. Ecol.: Prog. Ser.* **1995**, *123*, 301.
(5) Roberts, D.; Rittschof, D.; Holm, E.; Schmidt, A. R. Factors Influencing Initial Larval Settlement: Temporal, Spatial and Surface Molecular Components. *J. Exp. Mar. Biol. Ecol.* **1991**, *150*, 203−221.
(6) Wahl, M. Marine Epibiosis. I. Fouling and Antifouling: Some Basic Aspects. *Mar. Ecol.: Prog. Ser.* **1989**, *58*, 175−189.
(7) Mukhopadhyay, R. When Microfluidic Devices Go Bad. How Does Fouling Occur in Microfluidic Devices, and What Can Be Done about It? *Anal. Chem.* **2005**, *77*, 429A−432A.
(8) Delauney, L.; Compère, C.; Lehaitre, M. Biofouling Protection for Marine Environmental Sensors. *Ocean Sci.* **2010**, *6*, 503−511.
(9) Schultz, M. P. Effects of Coating Roughness and Biofouling on Ship Resistance and Powering. *Biofouling* **2007**, *23*, 331−341.
(10) Schultz, M. P.; Bendick, J. A.; Holm, E. R.; Hertel, W. M. Economic Impact of Biofouling on a Naval Surface Ship. *Biofouling* **2011**, *27*, 87−98.
(11) Otani, M.; Oumi, T.; Uwai, S.; Hanyuda, T.; Prabowo, R. E.; Yamaguchi, T.; Kawai, H. Occurrence and Diversity of Barnacles on International Ships Visiting Osaka Bay, Japan, and the Risk of Their Introduction. *Biofouling* **2007**, *23*, 277−286.
(12) Yamaguchi, T.; Prabowo, R. E.; Ohshiro, Y.; Shimono, T.; Jones, D.; Kawai, H.; Otani, M.; Oshino, A.; Inagawa, S.; Akaya, T.; Tamura, I. The Introduction to Japan of the Titan Barnacle, Megabalanus Coccopoma (Darwin, 1854) (Cirripedia: Balanomorpha) and the Role of Shipping in Its Translocation. *Biofouling* **2009**, *25*, 325−333.
(13) Pettengill, J. B.; Wendt, D. E.; Schug, M. D.; Hadfield, M. G. Biofouling Likely Serves as a Major Mode of Dispersal for the Polychaete Tubeworm Hydroides Elegans as Inferred from Microsatellite Loci. *Biofouling* **2007**, *23*, 161−169.
(14) Piola, R. F.; Johnston, E. L. The Potential for Translocation of Marine Species via Small-Scale Disruptions to Antifouling Surfaces. *Biofouling* **2008**, *24*, 145−155.
(15) Callow, J. A.; Callow, M. E. Trends in the Development of Environmentally Friendly Fouling-Resistant Marine Coatings. *Nat. Commun.* **2011**, *2*, 210−244.
(16) Barthlott, W.; Neinhuis, C. Purity of the Sacred Lotus, or Escape from Contamination in Biological Surfaces. *Planta* **1997**, *202*, 1−8.
(17) Burton, Z.; Bhushan, B. Surface Characterization and Adhesion and Friction Properties of Hydrophobic Leaf Surfaces. *Ultramicroscopy* **2006**, *106*, 709−719.
(18) Bhushan, B. Biomimetics: Lessons from Nature - an Overview. *Philos. Trans. R. Soc., A* **2009**, *367*, 1445−1486.
(19) Koch, K.; Barthlott, W. Superhydrophobic and Superhydrophilic Plant Surfaces: An Inspiration for Biomimetic Materials. *Philos. Trans. R. Soc., A* **2009**, *367*, 1487−1509.
(20) Bixler, G. D.; Theiss, A.; Bhushan, B.; Lee, S. C. Anti-Fouling Properties of Microstructured Surfaces Bio-Inspired by Rice Leaves and Butterfly Wings. *J. Colloid Interface Sci.* **2014**, *419*, 114−133.
(21) Bixler, G. D.; Bhushan, B. Rice and Butterfly Wing Effect Inspired Low Drag and Antifouling Surfaces: A Review. *Crit. Rev. Solid State Mater. Sci.* **2015**, *40*, 1−37.
(22) Wahl, M.; Kröger, K.; Lenz, M. Non-Toxic Protection against Epibiosis. *Biofouling* **1998**, *12*, 205−226.
(23) Stafford-Smith, M. G. Sediment-Rejection Mechanisms of 42 Species of Australian Scleractinian Corals. *Mar. Biol.* **1993**, *115*, 229−243.
(24) Ruppert, E. E.; Fox, R. S.; Barnes, R. D. *Invertebrate Zoology*, 7th ed.; Brooks Cole Thomson: Belmont, CA, 2004.
(25) Clifford, D. *Antony van Leeuwenhoek and His "Little Animals"*; Russel & Russel Publishers: New York, 1932.
(26) den Toonder, J. M. J.; Onck, P. R. *Artificial Cilia*; RSC Publishing: Cambridge, 2013.
(27) Blake, J. R.; Sleigh, M. A. Mechanism of Ciliary Locomotion. *Biol. Rev.* **1974**, *49*, 85−125.
(28) Fauci, L. J.; Dillon, R. Biofluidmechanics of Reproduction. *Annu. Rev. Fluid Mech.* **2006**, *38*, 371−394.
(29) Lyons, R. A.; Saridogan, E.; Djahanbakhch, O. The Reproductive Significance of Human Fallopian Tube Cilia. *Hum. Reprod. Update* **2006**, *12*, 363−372.
(30) Enuka, Y.; Hanukoglu, I.; Edelheit, O.; Vaknine, H.; Hanukoglu, A. Epithelial Sodium Channels (ENaC) Are Uniformly Distributed on Motile Cilia in the Oviduct and the Respiratory Airways. *Histochem. Cell Biol.* **2012**, *137*, 339−353.
(31) Sleigh, M. A. Adaptations of Ciliary Systems for the Propulsion of Water and Mucus. *Comp. Biochem. Physiol., Part A: Mol. Integr. Physiol.* **1989**, *94*, 359−364.
(32) Riisgård, H. U.; Larsen, P. S. Minireview: Ciliary Filter Feeding and Bio-Fluid Mechanics - Present Understanding and Unsolved Problems. *Limnol. Oceanogr.* **2001**, *46*, 882−891.
(33) Romero, M. R.; Kelstrup, H. C. P.; Strathmann, R. R. Capture of Particles by Direct Interception by Cilia during Feeding of a Gastropod Veliger. *Biol. Bull.* **2010**, *218*, 145−159.
(34) Labarbera, M. Feeding Currents and Particle Capture Mechanisms in Suspension Feeding Animals. *Am. Zool.* **1984**, *24*, 71−84.
(35) Taghon, G. L. Optimal Foraging by Deposit-Feeding Invertebrates: Roles of Particle Size and Organic Coating. *Oecologia* **1982**, *52*, 295−304.
(36) Jumars, P. A.; Self, R. F. l.; Nowell, A. R. M. Mechanics of Particle Selection by Tentaculate Deposit-Feeders. *J. Exp. Mar. Biol. Ecol.* **1982**, *64*, 47−70.
(37) Fritz, L. W.; Lutz, R. A.; Foote, M. A.; van Dover, C. L.; Ewart, J. W. Selective Feeding and Grazing Rates of Oyster (Crassostrea Virginica) Larvae on Natural Phytoplankton Assemblages. *Estuaries* **1984**, *7*, 513−518.
(38) Toonder, J. D.; Bos, F.; Broer, D.; Filippini, L.; Gillies, M.; De Goede, J.; Mol, T.; Reijme, M.; Talen, W.; Wilderbeek, H.; Khatavkar,

V.; Anderson, P. Artificial Cilia for Active Micro-Fluidic Mixing. *Lab Chip* **2008**, *8*, 533−541.
(39) Shields, A. R.; Fiser, B. L.; Evans, B. A.; Falvo, M. R.; Washburn, S.; Superfine, R. Biomimetic Cilia Arrays Generate Simultaneous Pumping and Mixing Regimes. *Proc. Natl. Acad. Sci. U.S.A.* **2010**, *107*, 15670−15675.
(40) Zhang, S.; Wang, Y.; Onck, P. R.; den Toonder, J. M. J. Removal of Microparticles by Ciliated Surfaces—an Experimental Study. *Adv. Funct. Mater.* **2019**, *29*, 1806434.
(41) Zhang, S.; Wang, Y.; Lavrijsen, R.; Onck, P. R.; den Toonder, J. M. J. Versatile Microfluidic Flow Generated by Moulded Magnetic Artificial Cilia. *Sens. Actuators, B* **2018**, *263*, 614−624.
(42) Van Oosten, C. L.; Bastiaansen, C. W. M.; Broer, D. J. Printed Artificial Cilia from Liquid-Crystal Network Actuators Modularly Driven by Light. *Nat. Mater.* **2009**, *8*, 677−682.
(43) Zarzar, L. D.; Kim, P.; Aizenberg, J. Bio-Inspired Design of Submerged Hydrogel-Actuated Polymer Microstructures Operating in Response to PH. *Adv. Mater.* **2011**, *23*, 1442−1446.
(44) Oh, K.; Chung, J.-H.; Devasia, S.; Riley, J. J. Bio-Mimetic Silicone Cilia for Microfluidic Manipulation. *Lab Chip* **2009**, *9*, 1561−1566.
(45) Gorissen, B.; De Volder, M.; Reynaerts, D. Pneumatically-Actuated Artificial Cilia Array for Biomimetic Fluid Propulsion. *Lab Chip* **2015**, *15*, 4348−4355.
(46) Toonder, J. M. J. d.; Onck, P. R. Microfluidic Manipulation with Artificial/Bioinspired Cilia. *Trends Biotechnol.* **2013**, *31*, 85−91.
(47) Khaderi, S. N.; Craus, C. B.; Hussong, J.; Schorr, N.; Belardi, J.; Westerweel, J.; Prucker, O.; Rühe, J.; Den Toonder, J. M. J.; Onck, P. R. Magnetically-Actuated Artificial Cilia for Microfluidic Propulsion. *Lab Chip* **2011**, *11*, 2002−2010.
(48) Wang, Y.; den Toonder, J.; Cardinaels, R.; Anderson, P. A Continuous Roll-Pulling Approach for the Fabrication of Magnetic Artificial Cilia with Microfluidic Pumping Capability. *Lab Chip* **2016**, *16*, 2277−2286.
(49) Chen, C.-Y.; Chen, C.-Y.; Lin, C.-Y.; Hu, Y.-T. Magnetically Actuated Artificial Cilia for Optimum Mixing Performance in Microfluidics. *Lab Chip* **2013**, *13*, 2834−2839.
(50) Hanasoge, S.; Hesketh, P. J.; Alexeev, A. Microfluidic Pumping Using Artificial Magnetic Cilia. *Microsyst. Nanoeng.* **2018**, *4*, 11.
(51) Khaderi, S. N.; Den Toonder, J. M. J.; Onck, P. R. Microfluidic Propulsion by the Metachronal Beating of Magnetic Artificial Cilia: A Numerical Analysis. *J. Fluid Mech.* **2011**, *688*, 44−65.
(52) Khaderi, S. N.; Baltussen, M. G. H. M.; Anderson, P. D.; den Toonder, J. M. J.; Onck, P. R. Breaking of Symmetry in Microfluidic Propulsion Driven by Artificial Cilia. *Phys. Rev. E: Stat., Nonlinear, Soft Matter Phys.* **2010**, *82*, 027302.
(53) Ghosh, R.; Buxton, G. A.; Usta, O. B.; Balazs, A. C.; Alexeev, A. Designing Oscillating Cilia That Capture or Release Microscopic Particles. *Langmuir* **2010**, *26*, 2963−2968.
(54) Branscomb, J.; Alexeev, A. Designing Ciliated Surfaces That Regulate Deposition of Solid Particles. *Soft Matter* **2010**, *6*, 4066−4069.
(55) Masoud, H.; Alexeev, A. Harnessing Synthetic Cilia to Regulate Motion of Microparticles. *Soft Matter* **2011**, *7*, 8702−8708.
(56) Dayal, P.; Kuksenok, O.; Bhattacharya, A.; Balazs, A. C. Chemically-Mediated Communication in Self-Oscillating, Biomimetic Cilia. *J. Mater. Chem.* **2012**, *22*, 241−250.
(57) Balazs, A. C.; Bhattacharya, A.; Tripathi, A.; Shum, H. Designing Bioinspired Artificial Cilia to Regulate Particle − Surface Interactions. *J. Phys. Chem. Lett.* **2014**, *5*, 1691−1700.
(58) Tripathi, A.; Shum, H.; Balazs, A. C. Fluid-Driven Motion of Passive Cilia Enables the Layer to Expel Sticky Particles. *Soft Matter* **2014**, *10*, 1416−1427.
(59) Zhang, S.; Wang, Y.; Onck, P.; den Toonder, J. A Concise Review of Microfluidic Particle Manipulation Methods. *Microfluid. Nanofluid.* **2020**, *24*, 24.
(60) Ben, S.; Tai, J.; Ma, H.; Peng, Y.; Zhang, Y.; Tian, D.; Liu, K.; Jiang, L. Cilia-Inspired Flexible Arrays for Intelligent Transport of Viscoelastic Microspheres. *Adv. Funct. Mater.* **2018**, *28*, 1706666.
(61) Gu, H.; Lee, S. W.; Carnicelli, J.; Zhang, T.; Ren, D. Magnetically Driven Active Topography for Long-Term Biofilm Control. *Nat. Commun.* **2020**, *11*, 1−11.
(62) Downton, M. T.; Stark, H. Beating Kinematics of Magnetically Actuated Cilia. *Epl* **2009**, *85*, 44002.
(63) Bruls, D. M.; Evers, T. H.; Kahlman, J. A. H.; Van Lankvelt, P. J. W.; Ovsyanko, M.; Pelssers, E. G. M.; Schleipen, J. J. H. B.; De Theije, F. K.; Verschuren, C. A.; Van Der Wijk, T.; Van Zon, J. B. A.; Dittmer, W. U.; Immink, A. H. J.; Nieuwenhuis, J. H.; Prins, M. W. J. Rapid Integrated Biosensor for Multiplexed Immunoassays Based on Actuated Magnetic Nanoparticles. *Lab Chip* **2009**, *9*, 3504−3510.
(64) Nie, C.; Frijns, A.; Zevenbergen, M.; den Toonder, J. M. J. An Integrated Flex-Microfluidic-Si Chip Device towards Sweat Sensing Applications. *Sens. Actuators, B* **2016**, *227*, 427−437.
(65) Khalili, A.; Ahmad, M. A Review of Cell Adhesion Studies for Biomedical and Biological Applications. *Int. J. Mol. Sci.* **2015**, *16*, 18149−18184.
(66) Wang, Y.; Gao, Y.; Wyss, H. M.; Anderson, P. D.; den Toonder, J. M. J. Artificial Cilia Fabricated Using Magnetic Fiber Drawing Generate Substantial Fluid Flow. *Microfluid. Nanofluid.* **2014**, *18*, 167−174.
(67) Wang, Y.; Gao, Y.; Wyss, H.; Anderson, P.; den Toonder, J. Out of the Cleanroom, Self-Assembled Magnetic Artificial Cilia. *Lab Chip* **2013**, *13*, 3360−3366.

https://dx.doi.org/10.1021/acsami.0c05403
ACS Appl. Mater. Interfaces 2020, 12, 27726−27736